Cooperative and non-cooperative sensitization upconversion in lanthanide-doped LiYbF₄ nanoparticles

- Supporting Information

Qilin Zou,[ab] Ping Huang,[a] Wei Zheng,[ab]* Wenwu You,[a] Renfu Li,[a] Datao Tu,[ab] Jin Xu,[a] and Xueyuan Chen[ab]*

[a]*CAS Key Laboratory of Design and Assembly of Functional Nanostructures, and State Key Laboratory of Structural Chemistry, Fujian Institute of Research on the Structure of Matter, Chinese Academy of Sciences, Fuzhou, Fujian 350002, China.*

[b]*College of Materials Science and Engineering, Fujian Normal University, Fuzhou, Fujian 350007, China.*

Fax: +86-591-63179421; Tel: +86-591-63179421; E-mail: xchen@fjirsm.ac.cn or zhengwei@fjirsm.ac.cn

Experimental Section

Chemicals and Materials: CH_3COOK, NH_4F, cyclohexane, methanol, and ethanol were purchased from Sinopharm Chemical Reagent Co., China. Oleic acid (OA) and trioctylamine (TOA) were purchased from Alfa Aesar (China). $Mg(CH_3COO)_2 \cdot 4H_2O$ (99.98%), $Ba(CH_3COO)_2$ (99.99%), $Yb(CH_3COO)_3 \cdot 4H_2O$ (99.999%) and $Er(CH_3COO)_3 \cdot 4H_2O$ (99.99%) were purchased from Sigma-Aldrich (China). All chemicals were used as received without further purification.

Synthesis of KMgF$_3$:Yb,Er core-only UCNPs: $KMgF_3$:Yb,Er core-only UCNPs were synthesized via a modified high-temperature co-precipitation method in the presence of OA and TOA as surfactant and solvent, respectively. In a typical synthesis of $KMgF_3$:18%Yb, 2%Er UCNPs, 1.5 mmol of CH_3COOK, 0.8 mmol of $Mg(CH_3COO)_2 \cdot 4H_2O$, 0.02 mmol of $Er(CH_3COO)_3 \cdot 4H_2O$, and 0.18 mmol of $Yb(CH_3COO)_3 \cdot 4H_2O$ were mixed with 6 mL of OA and 15 mL of TOA in a 100 mL three-neck round-bottom flask. The resulting mixture was heated to 160 °C under N_2 flow with constant stirring for 30 min to form a clear solution, and then cooled down to room temperature (RT). Thereafter, 10 mL of methanol solution containing 3 mmol of NH_4F was added and the solution was stirred at 60 °C for 30 min to remove methanol. After methanol was evaporated, the resulting solution was heated to 320 °C under N_2 flow with vigorous stirring for 60 min, and then cooled down to RT. The obtained UCNPs were precipitated by addition of 30 mL of ethanol, collected by centrifugation, washed with ethanol several times, and finally re-dispersed in cyclohexane.

Synthesis of KMgF$_3$:Yb,Er@KMgF$_3$ core/shell UCNPs: Briefly, 1.5 mmol of CH_3COOK and 1 mmol of $Mg(CH_3COO)_2 \cdot 4H_2O$ were added to a 100 mL three-neck round-bottom flask containing 6 mL of OA and 15 mL of TOA. The mixed solution was then heated to 160 °C under N_2 flow with constant stirring for 30 min to form a clear solution. After cooling down to 80 °C, 0.5 mmol of $KMgF_3$:Yb,Er core-only UCNPs in 10 mL of cyclohexane was added and maintained at 80 °C for 30 min to remove cyclohexane. After the removal of cyclohexane, 10 mL of methanol solution containing 3 mmol of NH_4F was added and stirred at 60 °C for another 30 min to remove methanol. After methanol was evaporated, the solution

was heated to 320 °C under N_2 flow with vigorous stirring for 60 min, and then cooled down to RT. The resulting core/shell UCNPs were precipitated by addition of 30 mL of ethanol, collected by centrifugation, washed with ethanol for several times, and finally re-dispersed in cyclohexane.

Synthesis of BaMgF₄:Yb,Er UCNPs: In a typical synthesis of $BaMgF_4$:18%Yb, 2%Er UCNPs, 0.8 mmol of $Ba(CH_3COO)_2$, 1 mmol of $Mg(CH_3COO)_2 \cdot 4H_2O$, 0.02 mmol of $Er(CH_3COO)_3 \cdot 4H_2O$, and 0.18 mmol of $Yb(CH_3COO)_3 \cdot 4H_2O$ were mixed with 8 mL of OA and 12 mL of TOA in a 100 mL three-neck round-bottom flask. The resulting mixture was heated to 240 °C under N_2 flow with constant stirring for 30 min to form a clear solution, and then cooled down to RT. Thereafter, 10 mL of methanol solution containing 4 mmol of NH_4F was added and the solution was stirred at 60 °C for 30 min to remove methanol. After methanol was evaporated, the resulting solution was heated to 330 °C under N_2 flow with vigorous stirring for 60 min, and then cooled down to RT. The obtained UCNPs were precipitated by addition of 30 mL of ethanol, collected by centrifugation, washed with ethanol several times, and finally re-dispersed in cyclohexane.

Determination of the absolute upconversion quantum yields (UCQYs): The absolute UCQYs were measured on a customized absolute UCQY measurement system combined with a fiber optic spectrometer (QE65pro, Ocean Optics), a standard barium sulfate coated integrating sphere (150 mm in diameter, Edinburgh Instruments), a 980-nm diode laser (MDL-Ⅲ-980-2W, Changchun New Industries Optoelectronics Tech Co., Ltd.) as the excitation source, and a neutral density filter to attenuate the excitation light (Fig. S1). The measurement was conducted deliberately according to the protocols reported by van Veggel and U. R. Genger *et al.*[1, 2] The integrating sphere was mounted on the optical platform with the entry and output ports of the sphere located in 90° geometry from each other. All the powder samples were mounted in a quartz cuvette located in the center of the integrating sphere. Pure $LiYbF_4$ nanocrystals for reference were mounted in another quartz cuvette in the integrating sphere with a distance of 2 cm away from the samples. Samples were excited with a 980-nm diode laser (MDL-Ⅲ-980-2W). An optical lens was used to collimate the laser beam and direct on the sample with a foucs of 1 mm²
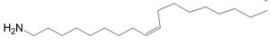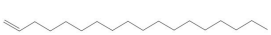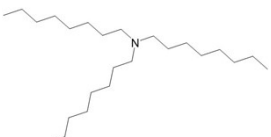
and a laser powermeter (Model 1918-C, Newport) was applied to measure the excitation power on the sample. The 980-nm absorption of the samples was measured by changing the position of the samples and the reference, and calculated by their difference in the corrected excitation spectra. Baffles were employed on both sides of the sample holder to ensure that no scattered excitation light or emissions would be collected before scattering off the inside of the sphere. All the spectroscopic data collected were corrected for both the spectral response of both the spectrometer and the integrating sphere. The response of the detection systems in photon flux (integrating sphere, monochromators, and detectors) was determined using a calibrated tungsten lamp (100 W, Edinburgh Instruments). The normalization curves were then applied to all measured spectra. The UCQYs were then calculated by[1]

$$QY = \frac{N_e}{N_a} = \frac{L_s}{E_R - E_S}$$

where N_e and N_a are the photons emitted and absorbed, respectively; L_s is the emission intensity, E_R and E_S are the intensities of the excitation light in the presence of the pure $LiYbF_4$ nanocrystals (reference) and the UCNP samples, respectively. The UCL emission peaks in the spectral region of 460-620 nm for Tb^{3+}, 410-690 nm for Er^{3+}, 330-840 nm for Tm^{3+} and 470-630 nm for Ho^{3+} were integrated for the QY determination. All the UCQYs for each sample were measured independently for at least five times under identical conditions to yield the average value and standard deviation.

Table S1. Comparison of the physicochemical properties of OA,[3] oleylamine (OM),[3] 1-octadecence (ODE), and TOA[4] used in the synthesis of Ln^{3+}-doped UCNPs.

Solvent	CAS number	Molecular formula	Structural formula	Boiling point / °C	Density / g/mL (25 °C)	Viscosity / mPa·s
OA	112-80-1	$C_{18}H_{34}O_2$		360	0.89	36 (25 °C)
OM	112-90-3	$C_{18}H_{37}N$		348-350	0.81	161 (25 °C)
ODE	112-88-9	$C_{18}H_{36}$		314.2	0.79	2.84 (40 °C)
TOA	1116-76-3	$C_{24}H_{51}N$		365.8	0.81	8.33 (23°C)

Table S2. Absolute UCQYs of $LiYbF_4:Ln^{3+}@LiYF_4$ core/shell UCNPs upon 980-nm NIR laser excitation at a power density of 70 $W \cdot cm^{-2}$. Each UCQY value represents the average ($\pm$ standard deviation) of five independent measurements under identical conditions.

Sample	Size (nm)	UCQY
$LiYbF_4:2\%Er@ LiYF_4$	30	3.36 ± 0.06 %
$LiYbF_4:2\%Ho@ LiYF_4$	30	0.69 ± 0.01 %
$LiYbF_4:1\%Tm@ LiYF_4$	30	0.81 ± 0.06 %
$LiYbF_4:30\%Tb@ LiYF_4$	26	0.0085 ± 0.0035 %

Table S3. Temperature-dependent UCL lifetimes of $^5D_4$ of Tb^{3+} in $LiYbF_4$:30%Tb@$LiYF_4$ core/shell UCNPs upon excitation at 980 nm. τ_{rise} and τ_{decay} represent the rise time and decay time, respectively. The experimental errors were determined to be smaller than 0.01 ms for both the rise time and decay time.

T (K)	10	30	50	70	100	150	200	250	300
τ_{rise} (ms)	None	None	0.43	0.50	0.70	0.84	0.83	0.82	0.76
τ_{decay} (ms)	6.53	6.63	6.84	6.97	6.92	6.84	6.63	6.44	6.39

References:

1. J.-C. Boyer and F. C. J. M. van Veggel, *Nanoscale* **2010**, *2*, 1417.

2. C. Würth, M. Grabolle, J. Pauli, M. Spieles, and U. Resch-Genger, *Nat. Protoc.* **2013**, *8*, 1535.

3. Y. J. Shi and R. Larsson, *Tribol. Lett.* **2016**, *63*, 1.

4. M. Roos and H. J. Bart, *J. Chem. Eng. Data* **2001**, *46,* 1198.
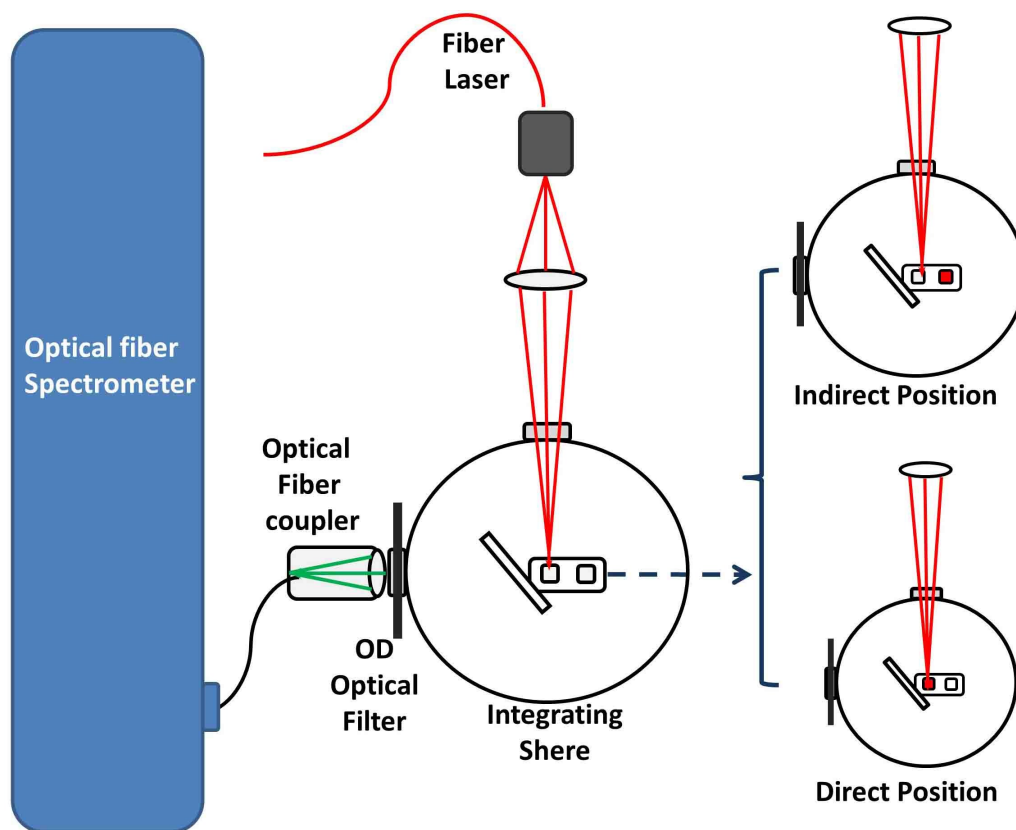
Figure S1. Schematic illustration of the configuration of the customized absolute UCQY measurement system.
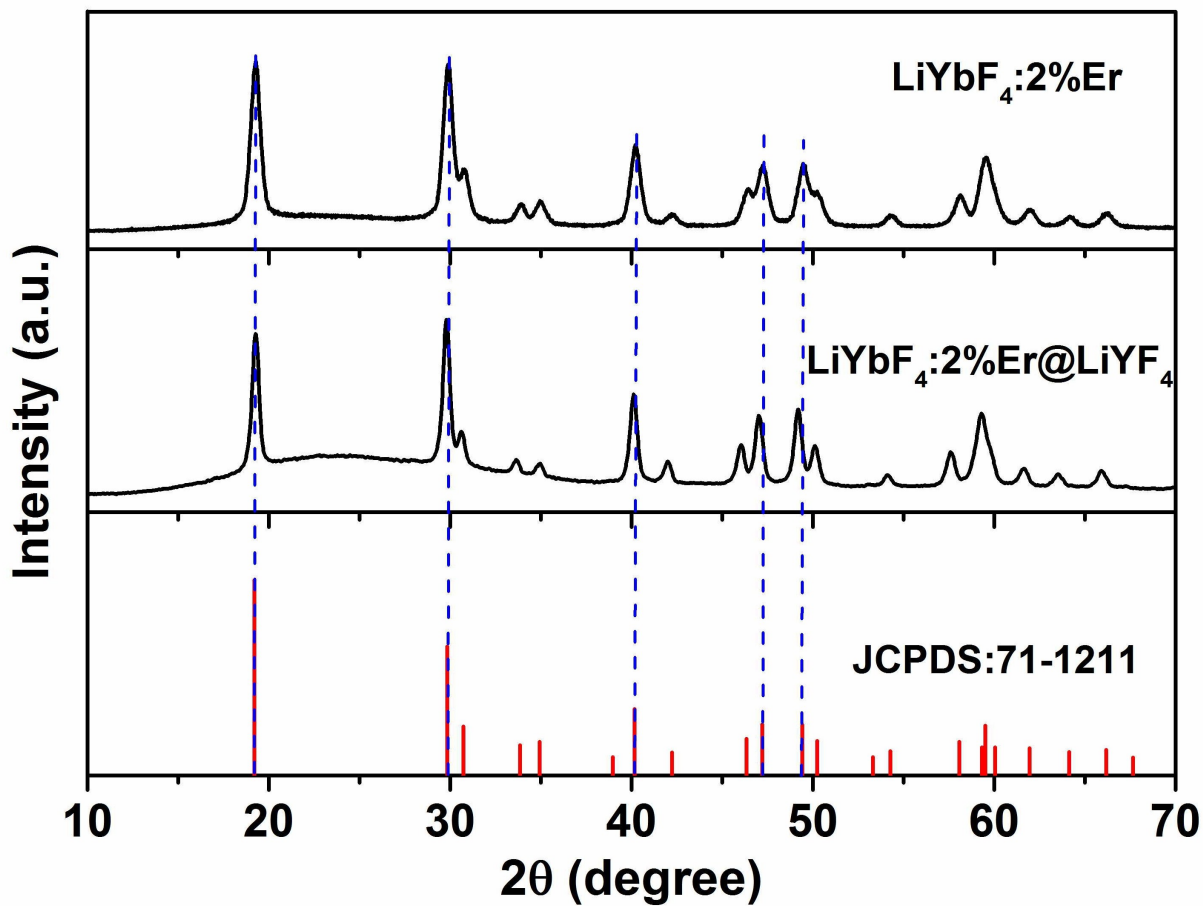
Figure S2. XRD patterns of LiYbF$_4$:2%Er core-only and LiYbF$_4$:2%Er@LiYF$_4$ core/shell UCNPs. All diffraction peaks match well with the standard pattern of tetragonal-phase LiYbF$_4$ (JCPDS No. 71-1211), indicating the pure phase and the high crystallinity of the UCNPs.
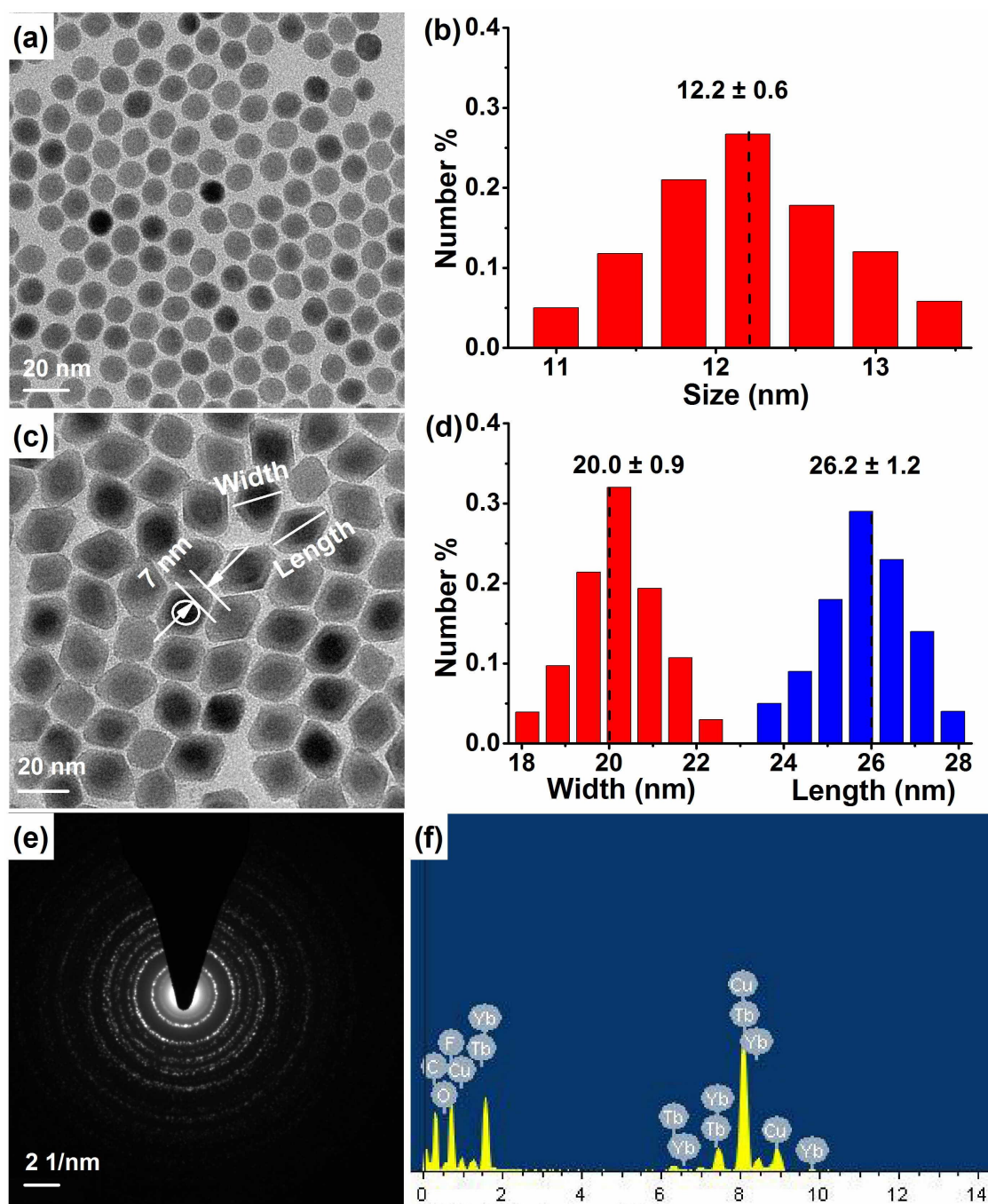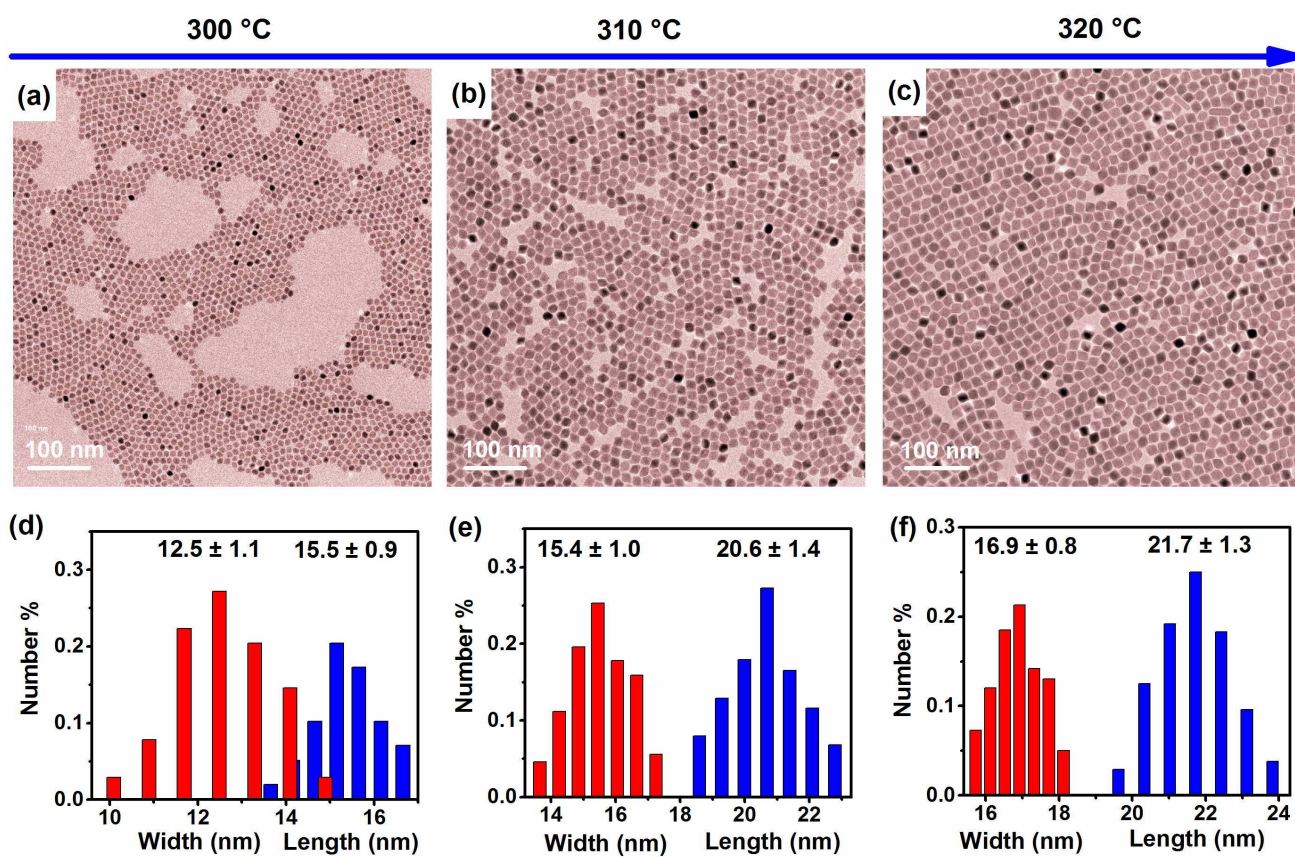
Figure S3. TEM images and size distributions of (a, b) LiYbF$_4$:30%Tb core-only and (c, d) LiYbF$_4$:30%Tb@LiYF$_4$ core/shell UCNPs. (e) Selected area electron diffraction (SAED) pattern showing the high crystallinity of LiYbF$_4$:30%Tb UCNPs. (f) Energy dispersive X-ray spectrum (EDS) pattern showing the elements of Yb, Tb and F in LiYbF$_4$:30%Tb UCNPs. The size distributions were obtained by calculating 200 particles in the TEM images.
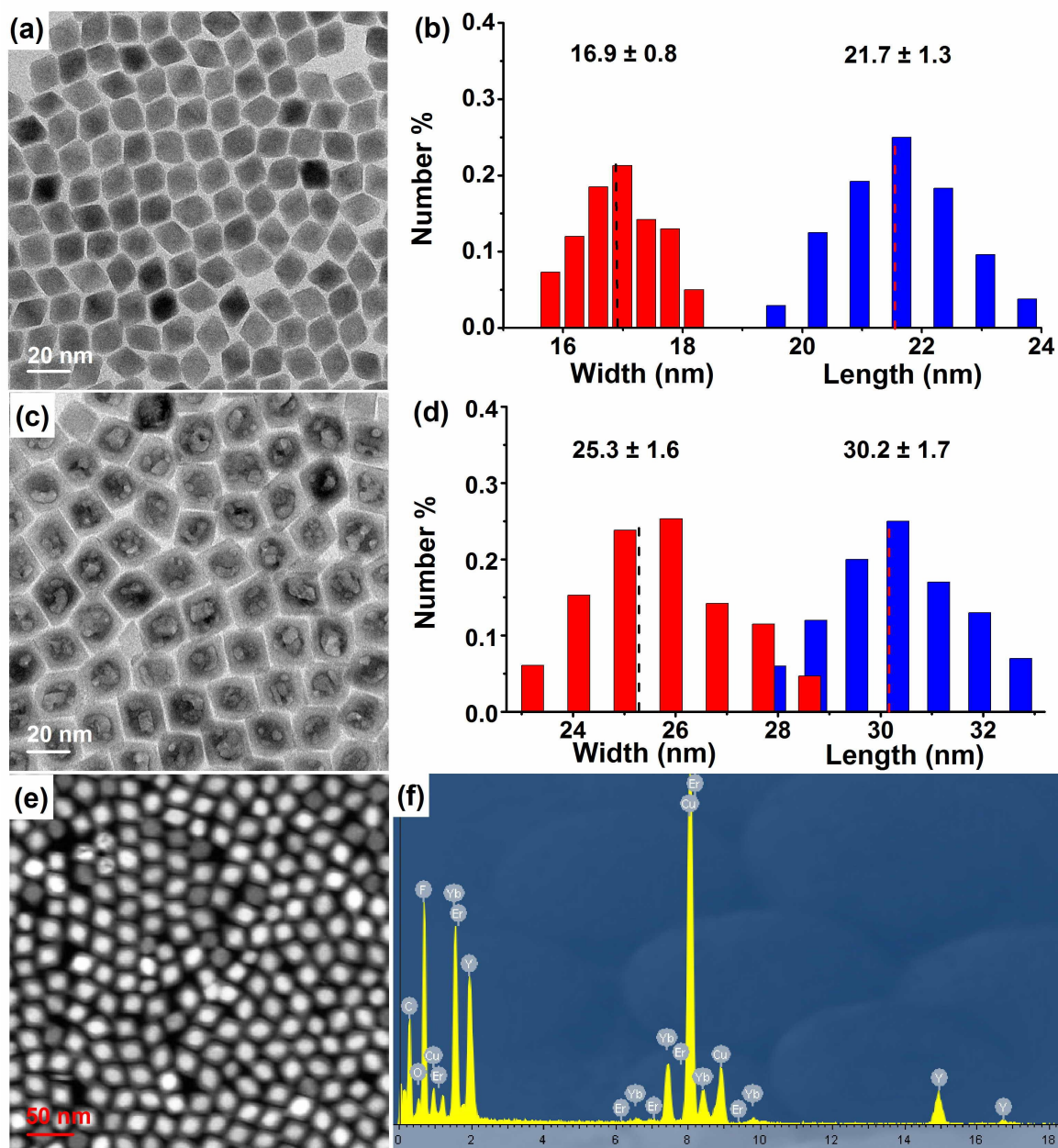
Figure S4. TEM images and size distributions of (a, b) LiYbF$_4$:2%Er core-only and (c, d) LiYbF$_4$:2%Er@LiYF$_4$ core/shell UCNPs. (e) High-angle annular dark-field scanning TEM (HAADF-STEM) image of LiYbF$_4$:2%Er@LiYF$_4$ core/shell UCNPs, where the brighter regions correspond to the heavier Yb^{3+} ions in the cores, and the darker regions correspond to the lighter Y^{3+} ions in the shells. (f) EDS pattern showing the elements of Yb, Er, Y and F in LiYbF$_4$:2%Er@LiYF$_4$ core/shell UCNPs.

Figure S5. TEM images and size distributions of LiYbF$_4$:2%Er UCNPs synthesized at (a, d) 300 °C, (b, e) 310 °C and (c, f) 320 °C for 1 h.
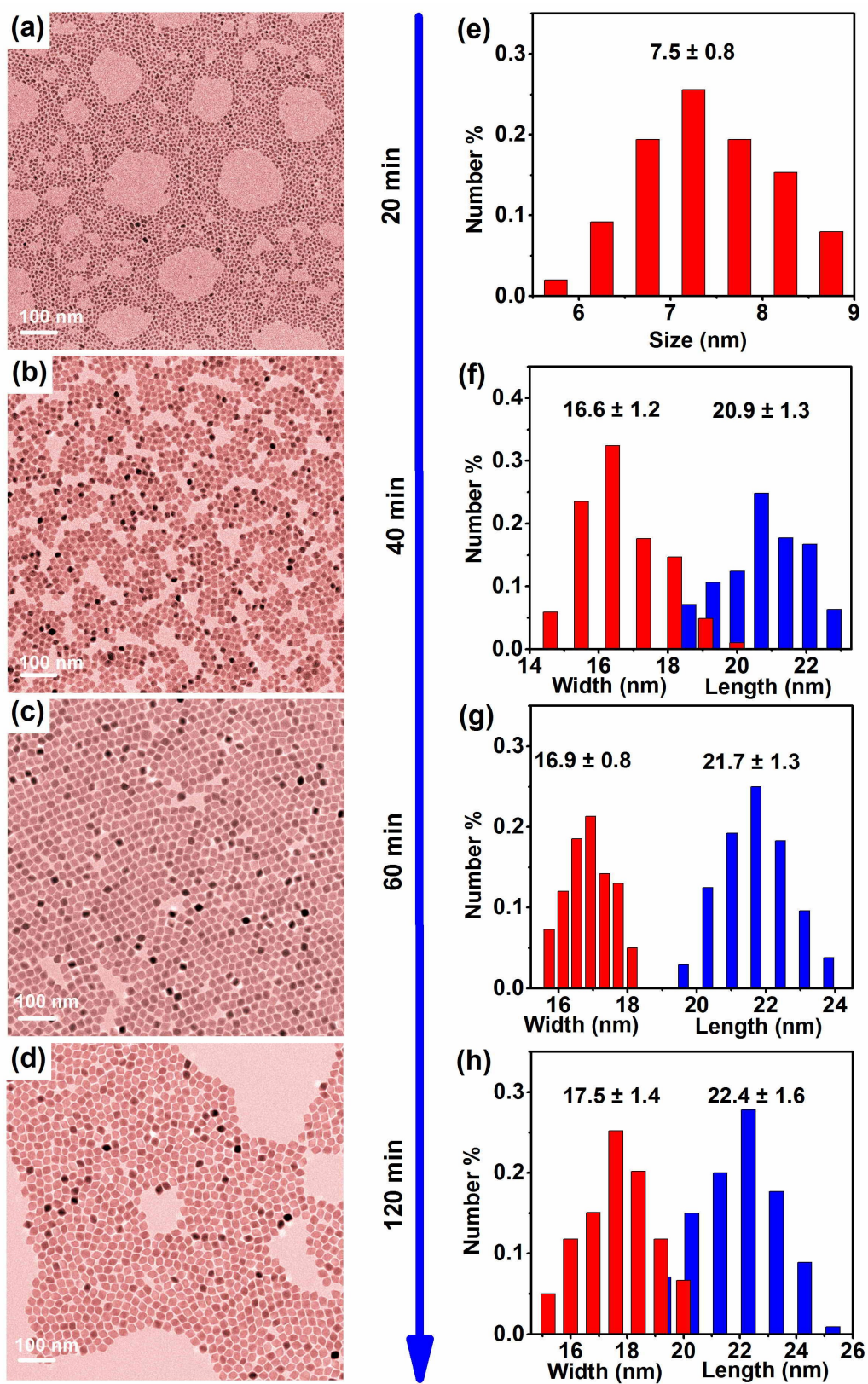
Figure S6. TEM images and size distributions of LiYbF$_4$:2%Er UCNPs synthesized at 320 °C for (a, e) 20 min, (b, f) 40 min, (c, g) 60 min and (d, h) 120 min.
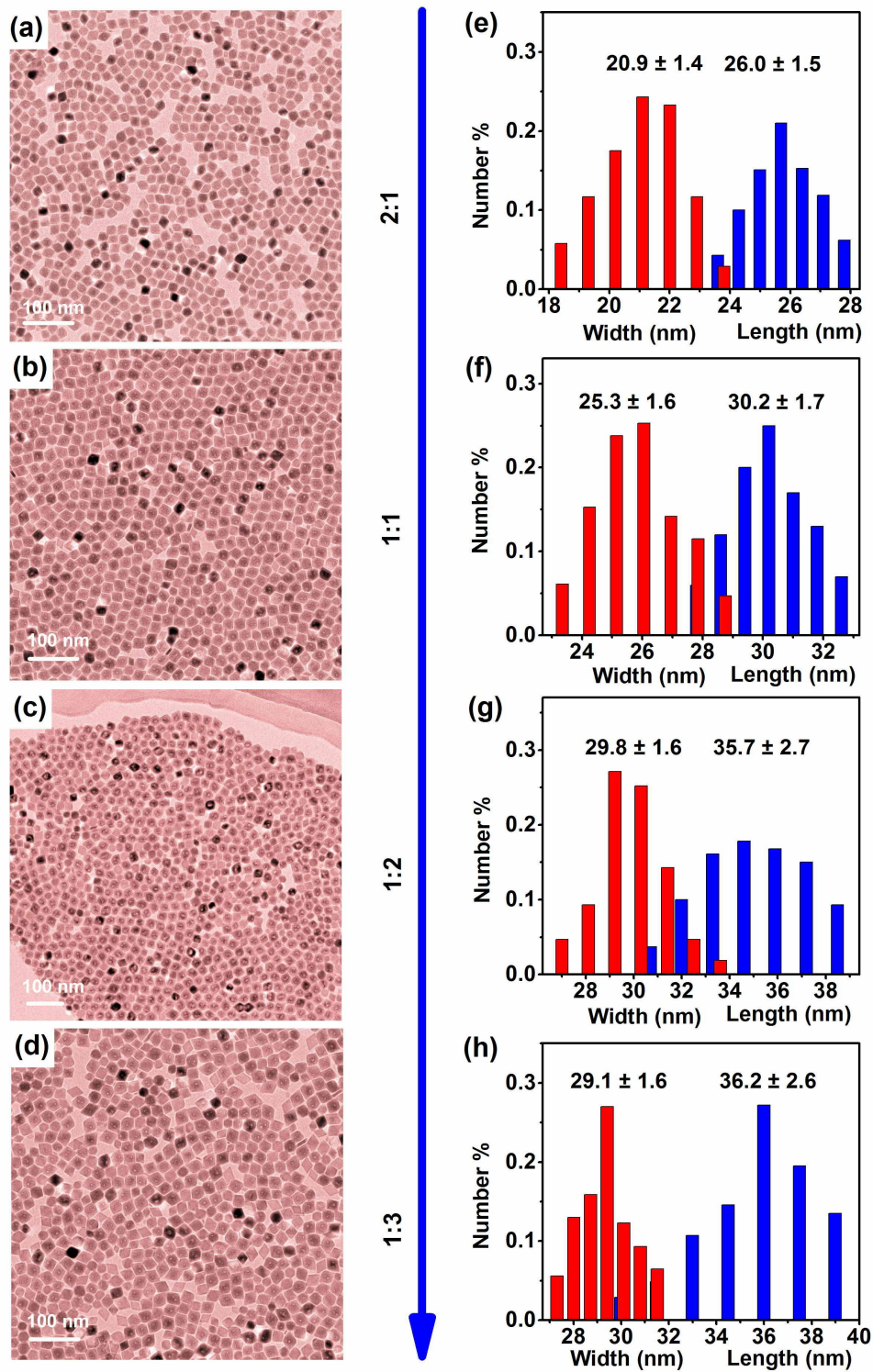
Figure S7. TEM images and size distributions of LiYbF$_4$:2%Er@LiYF$_4$ core/shell UCNPs synthesized with core/shell precursor ratio of (a, e) 2:1, (b, f) 1:1, (c, g) 1:2 and (d, h) 1:3. Through the control of the core/shell precursor ratio, the shell thickness of the UCNPs can be tuned from 2 nm to 7 nm (in length).
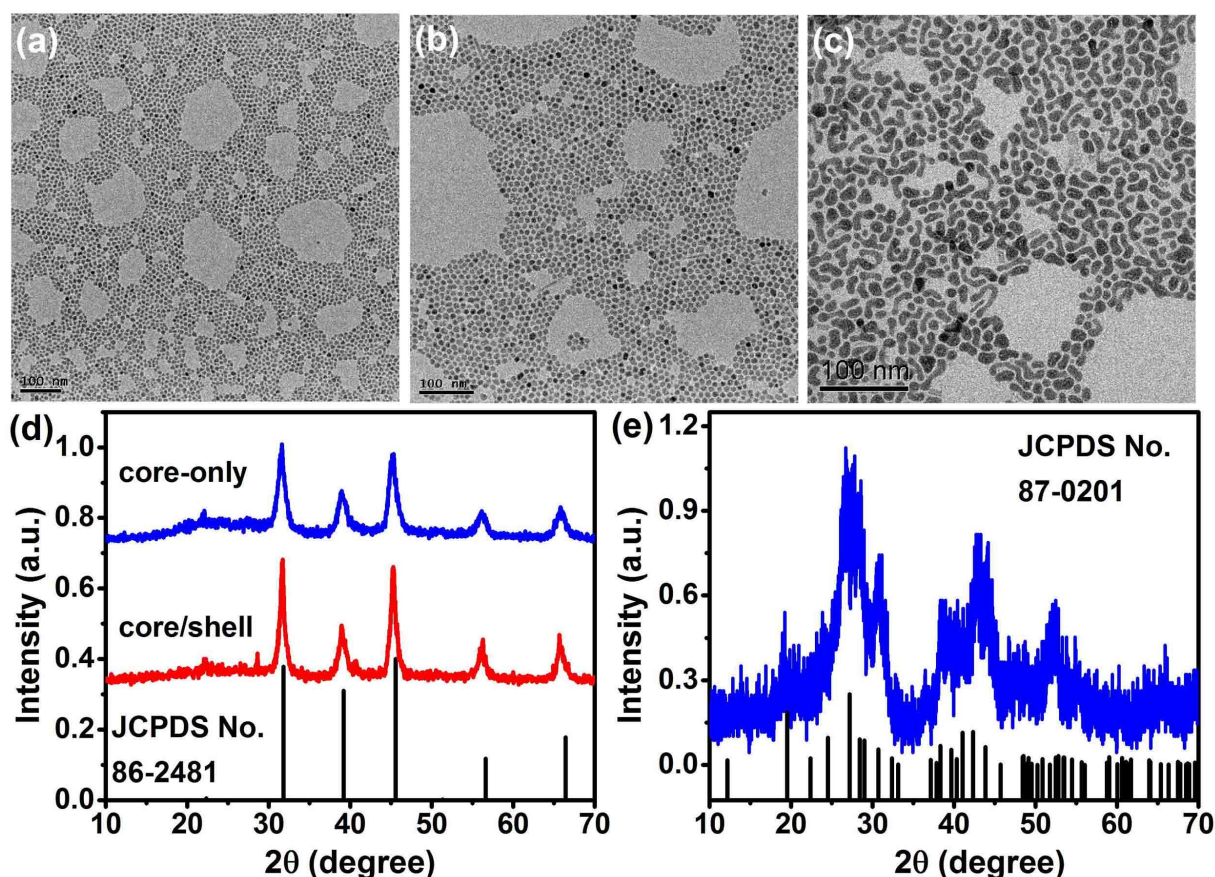
Figure S8. TEM images of (a) KMgF$_3$:Yb,Er core-only, (b) KMgF$_3$:Yb,Er@KMgF$_3$ core/shell, and (c) BaMgF$_4$:Yb,Er UCNPs. XRD patterns of (d) KMgF$_3$:Yb,Er core-only, KMgF$_3$:Yb,Er@KMgF$_3$ core/shell, and (e) BaMgF$_4$:Yb,Er UCNPs. The bottom lines in (d) and (e) show the standard XRD patterns of cubic KMgF$_3$ (JCPDS No. 86-2481) and orthorhombic BaMgF$_4$ (JCPDS No. 87-0201). TEM images shows that both KMgF$_3$:Yb,Er core-only and core/shell UCNPs are roughly spherical with their mean sizes of (8.6 ± 0.4) nm and (12.5 ± 0.6) nm, respectively; while BaMgF$_4$:Yb,Er UCNPs exhibit a wormy-like morphology with a mean size smaller than 30 nm. XRD patterns show that all the diffraction peaks of both KMgF$_3$:Yb,Er core-only and core/shell UCNPs can be well indexed into cubic KMgF$_3$ (JCPDS No. 86-2481), and the diffraction peaks of BaMgF$_4$:Yb,Er UCNPs can be indexed into orthorhombic BaMgF$_4$ (JCPDS No. 87-0201), indicating the pure phase and the high crystallinity of the UCNPs. Upon 980-nm excitation, KMgF$_3$:Yb,Er and BaMgF$_4$:Yb,Er UCNPs displayed red and green UCL, respectively (unpublished data).
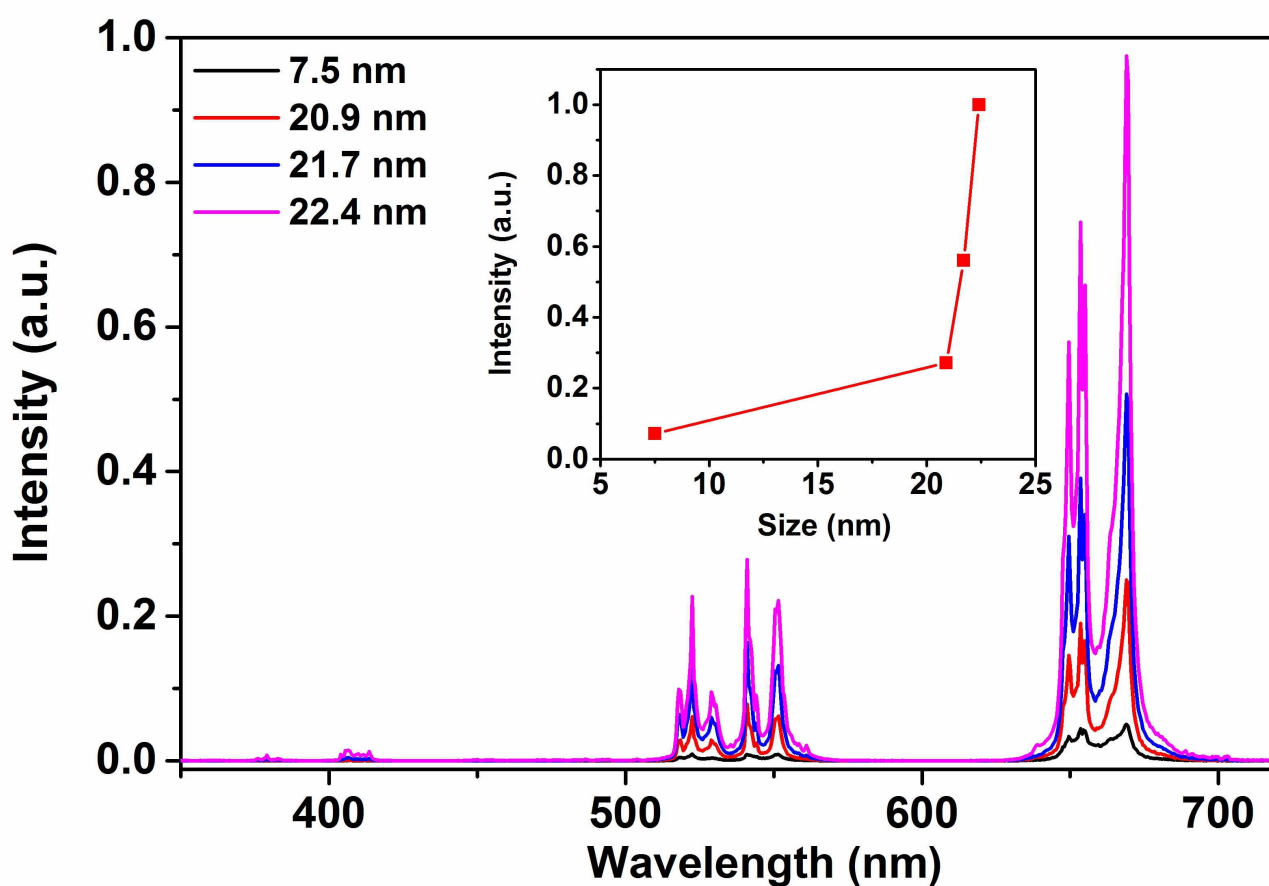
Figure S9. UCL spectra of LiYbF$_4$:2%Er UCNPs with different NP size (in length) under 980-nm excitation. The inset shows the integrated UCL intensity of the UCNPs as a function of NP size. The integrated UCL intensity of the UCNPs was gradually enhanced with the increase in the particle size due to the reduced surface quenching effect. Typically, the integrated UCL intensity of the UCNPs was remarkably enhanced by a factor of 14 upon increasing their particle size from ~7.5 nm to ~(17.5 × 22.4) nm.
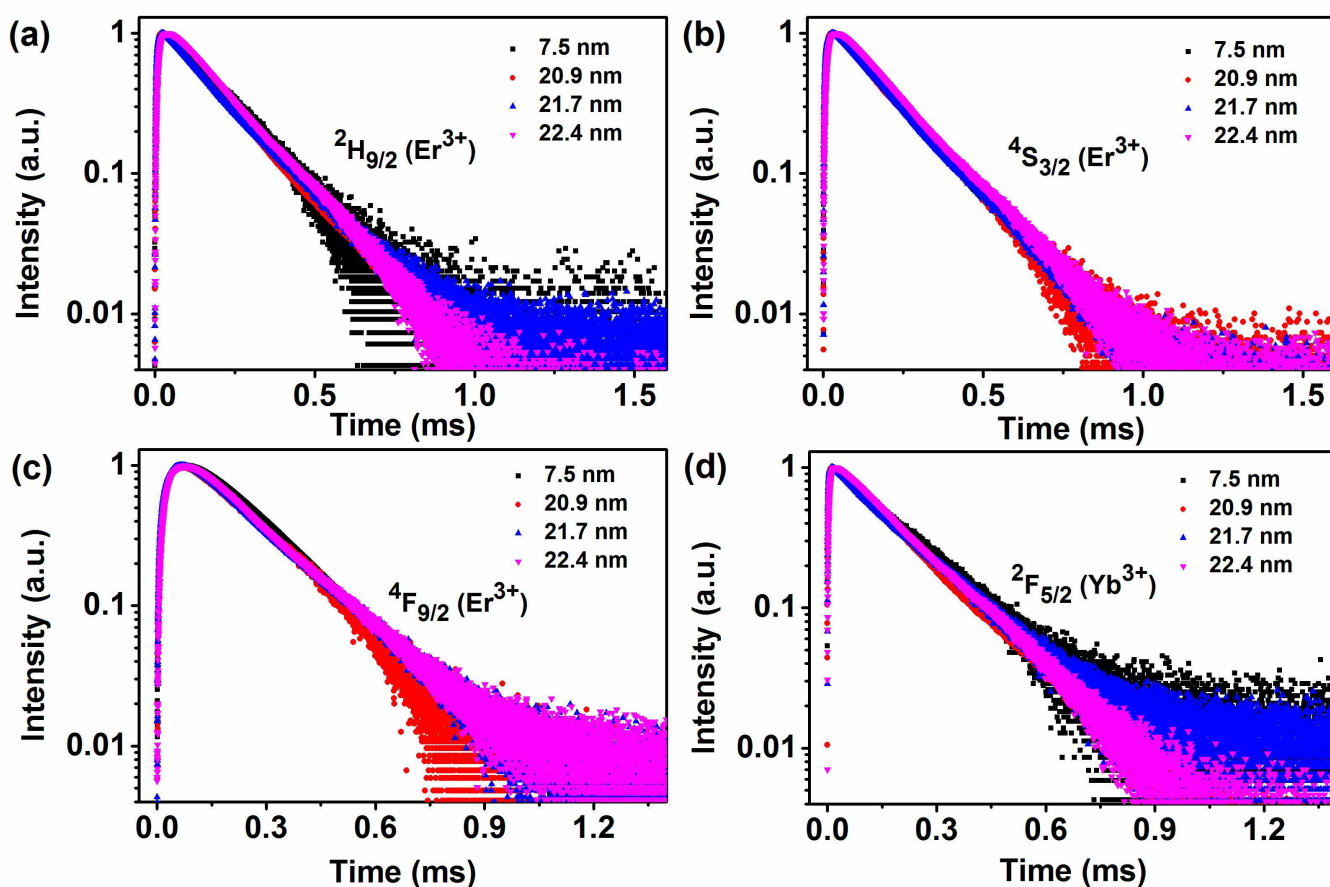
Figure S10. UCL lifetimes of (a) $^2H_{9/2}$, (b) $^4S_{3/2}$ and (c) $^4F_{9/2}$ of Er^{3+} in $LiYbF_4$:2%Er UCNPs with different NP size under 980-nm excitation. (d) DSL lifetimes of $^2F_{5/2}$ of Yb^{3+} under 940-nm excitation. All the PL lifetimes of Er^{3+} and Yb^{3+} exhibit a single-exponential decay and are nearly identical for UCNPs with different NP size. Through the single-exponential fitting to the decays, the UCL lifetimes of $^2H_{9/2}$, $^4S_{3/2}$ and $^4F_{9/2}$ of Er^{3+} were determined to be 0.17, 0.17 and 0.19 ms, respectively; and the DSL lifetime of $^2F_{5/2}$ of Yb^{3+} was determined to be 0.18 ms. The experimental errors for both the UCL and DSL lifetimes were smaller than 0.01 ms.
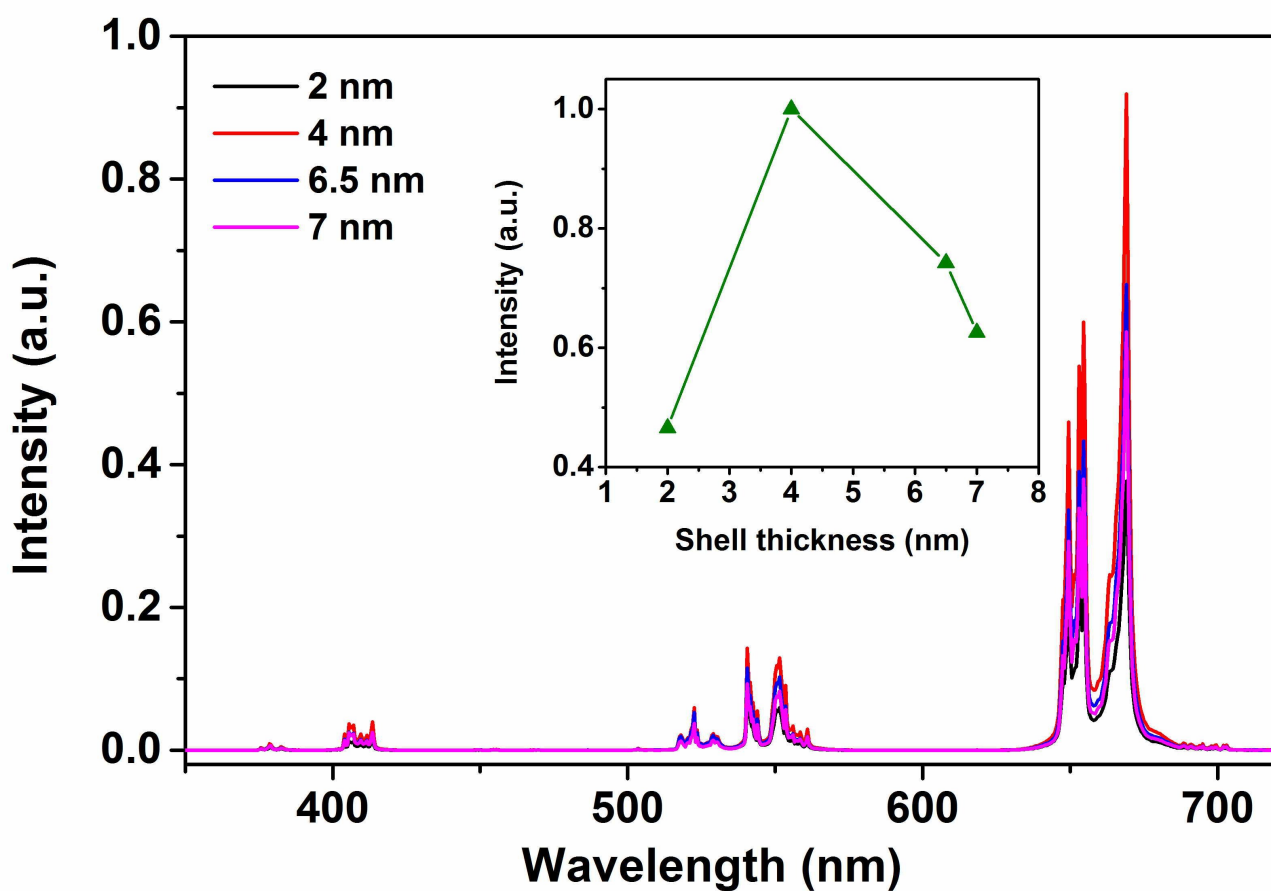
Figure S11. UCL spectra of $LiYbF_4$:2%Er@$LiYF_4$ core/shell UCNPs with different shell thickness under 980-nm excitation. The inset shows the integrated UCL intensity of the UCNPs as a function of shell thickness. The integrated UCL intensity of the core/shell UCNPs undergoes an initial increase and then decreases with the increase in the shell thickness. This can be attributed to a synergic effect of the increased isolation of the core from its environment and the decreased Yb^{3+} absorption arising from the increased shell thickness.
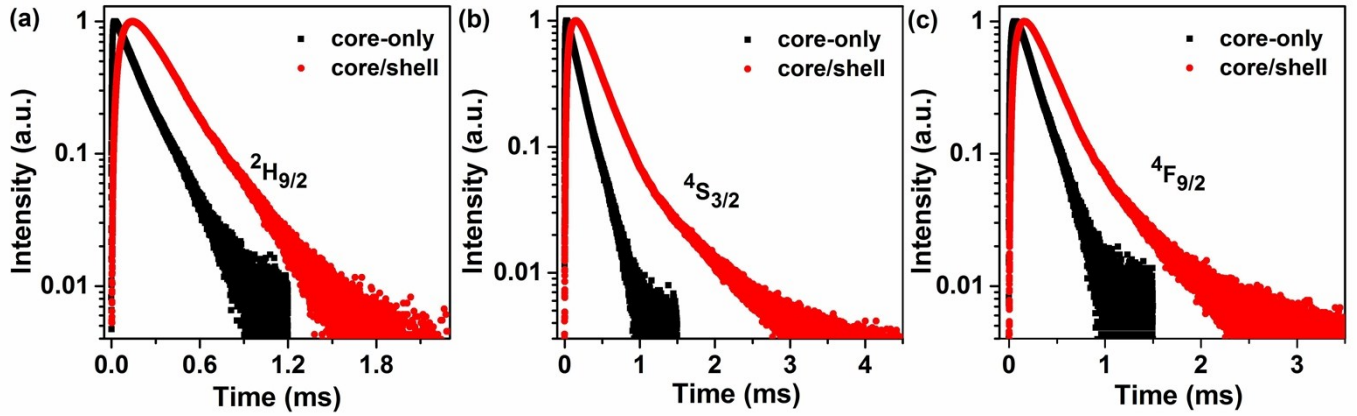
Figure S12. UCL lifetimes of (a) $^2H_{9/2}$, (b) $^4S_{3/2}$ and (c) $^4F_{9/2}$ of Er^{3+} in $LiYbF_4$:2%Er core-only and $LiYbF_4$:2%Er@$LiYF_4$ core/shell UCNPs with optimal shell thickness. The UCL lifetimes were determined by single-exponential fit to the decays. For non-exponential decay, the effective UCL lifetime was calculated by

$$\tau_{eff} = \frac{1}{I_{max}} \int_0^\infty I(t)dt$$

where $I(t)$ denotes the UCL intensity as a function of time t, and I_{max} represents the maximum UCL intensity. The UCL lifetimes of $^2H_{9/2}$, $^4S_{3/2}$ and $^4F_{9/2}$ of Er^{3+} were determined to increase from 0.17, 0.17 and 0.19 ms in core-only UCNPs to 0.30, 0.36 and 0.35 ms in core/shell UCNPs, respectively. The experimental errors for the UCL lifetimes were smaller than 0.01 ms.
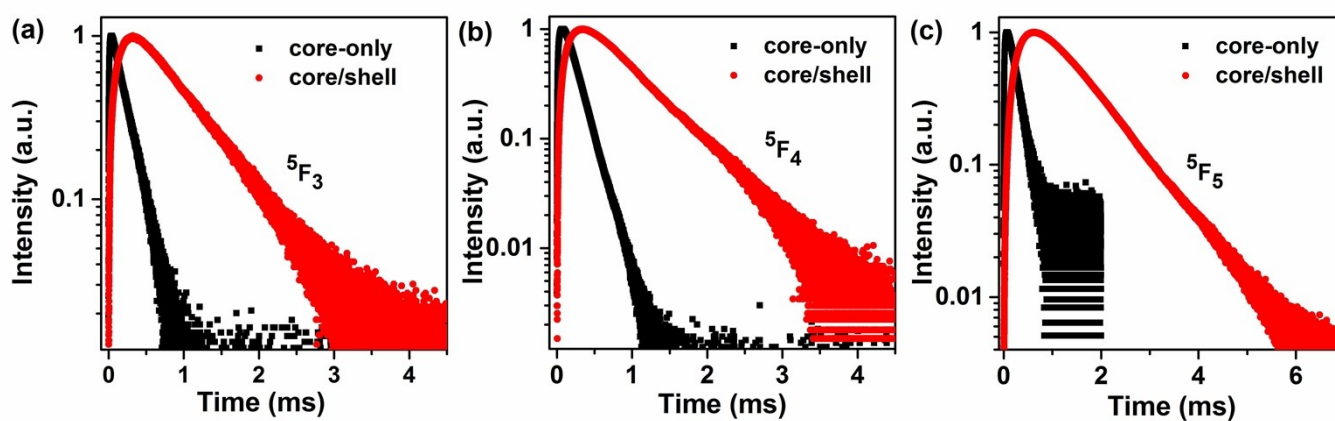
Figure S13. UCL lifetimes of (a) $^5F_3$, (b) $^5F_4$ and (c) $^5F_5$ of Ho^{3+} in $LiYbF_4$:2%Ho core-only and $LiYbF_4$:2%Ho@$LiYF_4$ core/shell UCNPs with optimal shell thickness. All the UCL lifetimes of Ho^{3+} exhibit a single-exponential decay with fitted lifetimes increasing from 0.20, 0.17 and 0.21 ms in core-only UCNPs to 0.74, 0.64 and 1.00 ms in core/shell UCNPs for $^5F_3$, $^5F_4$ and $^5F_5$, respectively. The experimental errors for the UCL lifetimes were smaller than 0.01 ms.
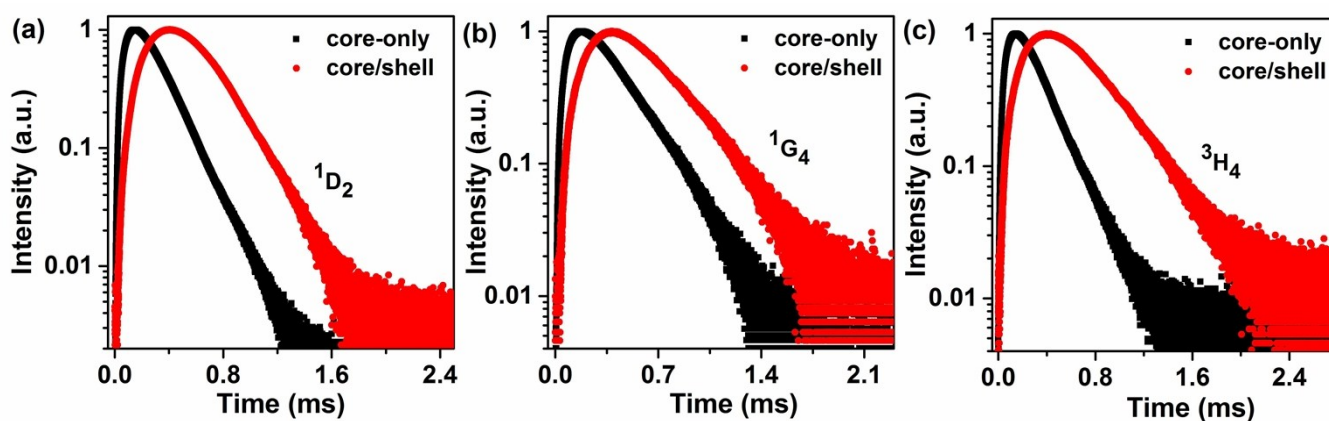
Figure S14. UCL lifetimes of (a) $^1D_2$, (b) $^1G_4$ and (c) $^3H_4$ of Tm^{3+} in $LiYbF_4$:1%Tm core-only and $LiYbF_4$: 1%Tm@$LiYF_4$ core/shell UCNPs with optimal shell thickness. The UCL lifetimes of $^1D_2$, $^1G_4$ and $^3H_4$ of Tm^{3+} were determined to increase from 0.19, 0.29 and 0.20 ms in core-only UCNPs to 0.43, 0.46 and 0.54 ms in core/shell UCNPs, respectively. The experimental errors for the UCL lifetimes were smaller than 0.01 ms.
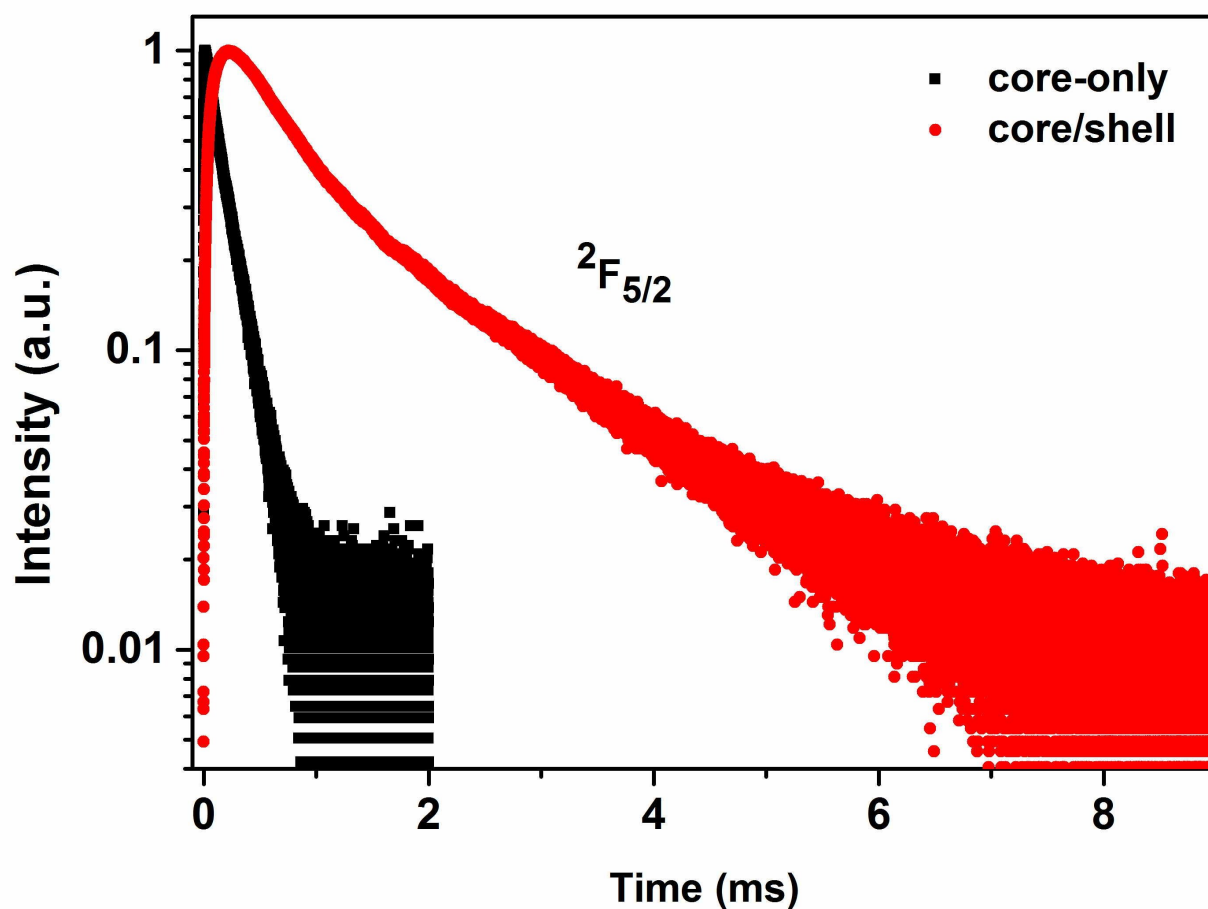
Figure S15. DSL lifetimes of $^2F_{5/2}$ of Yb^{3+} in $LiYbF_4$:2%Er core-only and $LiYbF_4$:2%Er@$LiYF_4$ core/shell UCNPs with optimal shell thickness. The DSL lifetime of $^2F_{5/2}$ of Yb^{3+} was determined to increase from 0.18 ms in core-only UCNPs to 1.2 ms in core/shell UCNPs. The significantly lengthened lifetime of Yb^{3+} demonstrates the effective surface passivation of the core/shell UCNPs which alliviates the deleterious suface quenching effect arsing from energy migration through Yb^{3+} sub-lattice to surface defects or high-energy vibrational groups surrounded the UCNPs. The experimental errors for the DSL lifetimes were smaller than 0.01 ms.
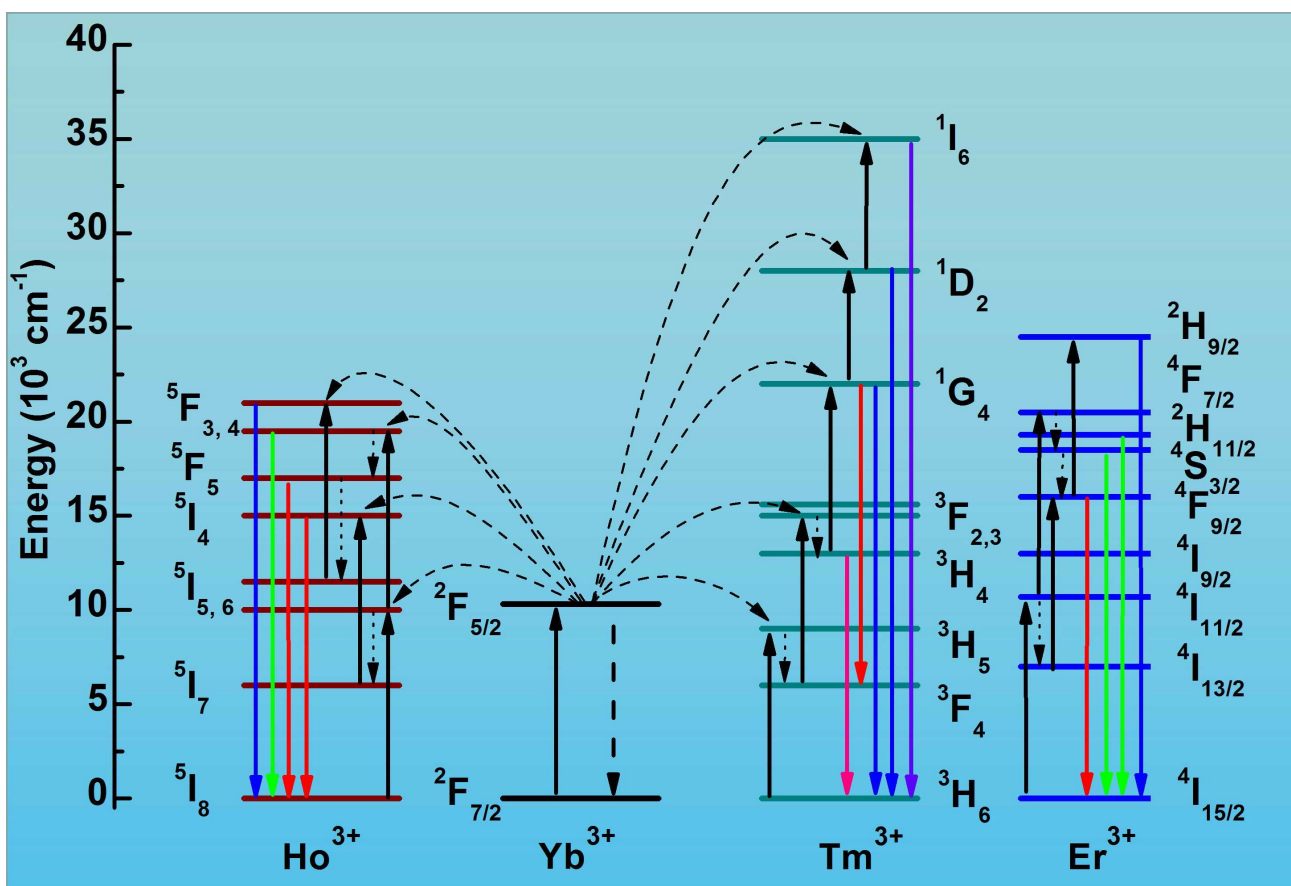
Figure S16. Schematic energy level diagrams showing the energy transfer UC processes for Ho^{3+}, Tm^{3+} and Er^{3+} via the non-cooperative sensitization of Yb^{3+}. The dashed, dotted and full arrows represent the energy transfer, non-radiative relaxation and radiative transition processes, respectively.
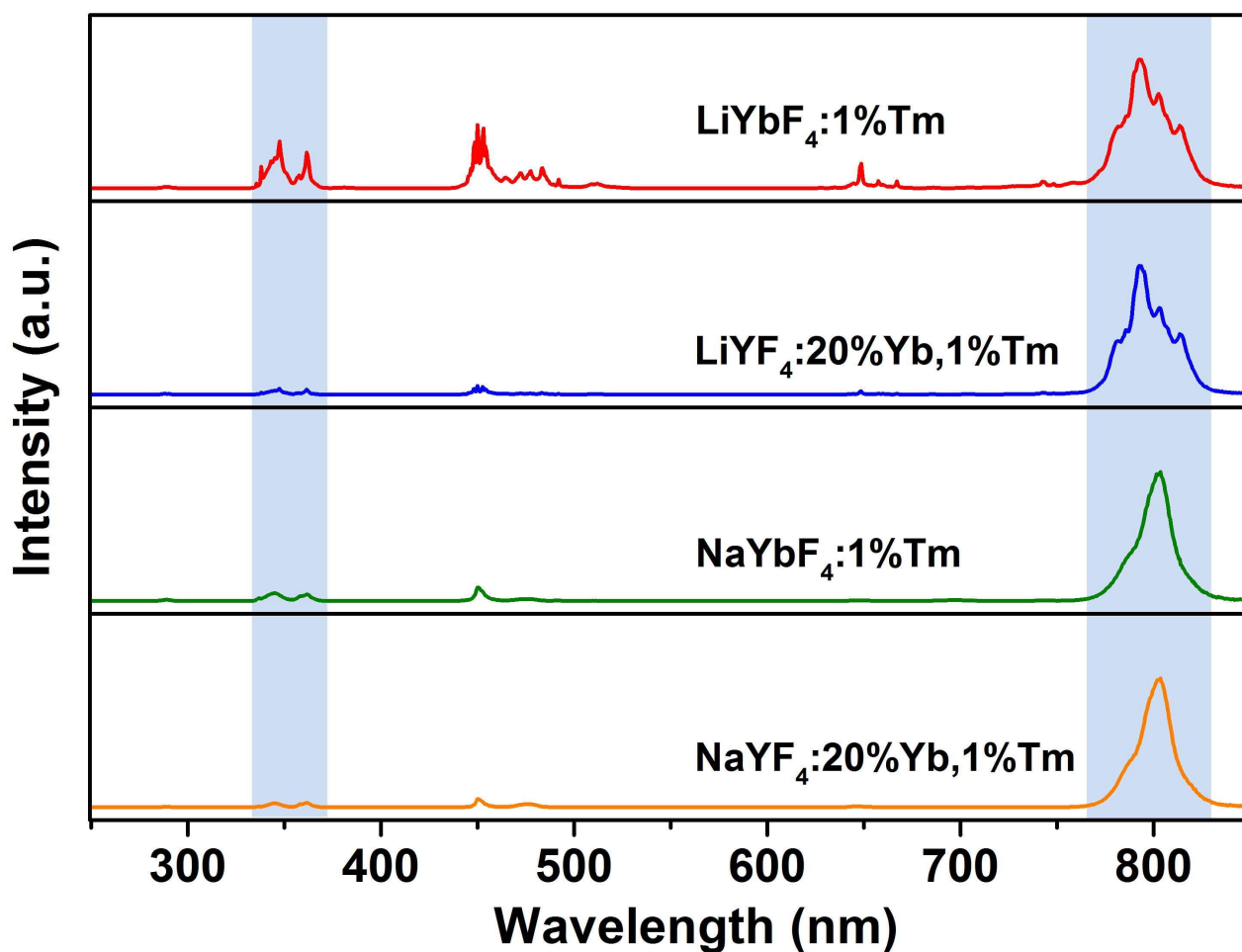
Figure S17. Comparison of the UCL spectra of $LiYbF_4$:Tm, $LiYF_4$:Yb,Tm, $NaYbF_4$:Tm and $NaYF_4$:Yb,Tm UCNPs with similar particle size upon 980-nm NIR excitation at a power density of 5 $W \cdot cm^{-2}$. $LiYF_4$:Yb,Tm, $NaYbF_4$:Tm and $NaYF_4$:Yb,Tm UCNPs were synthesized according to our previously reported methods. The ratio of the integrated UCL intensity of the UV emission at ~362 nm to the NIR emission at ~800 nm ($R_{UV/NIR}$) was determined to be 0.14, 0.01, 0.02 and 0.01 for $LiYbF_4$:Tm, $LiYF_4$:Yb,Tm, $NaYbF_4$:Tm and $NaYF_4$:Yb,Tm, respectively.
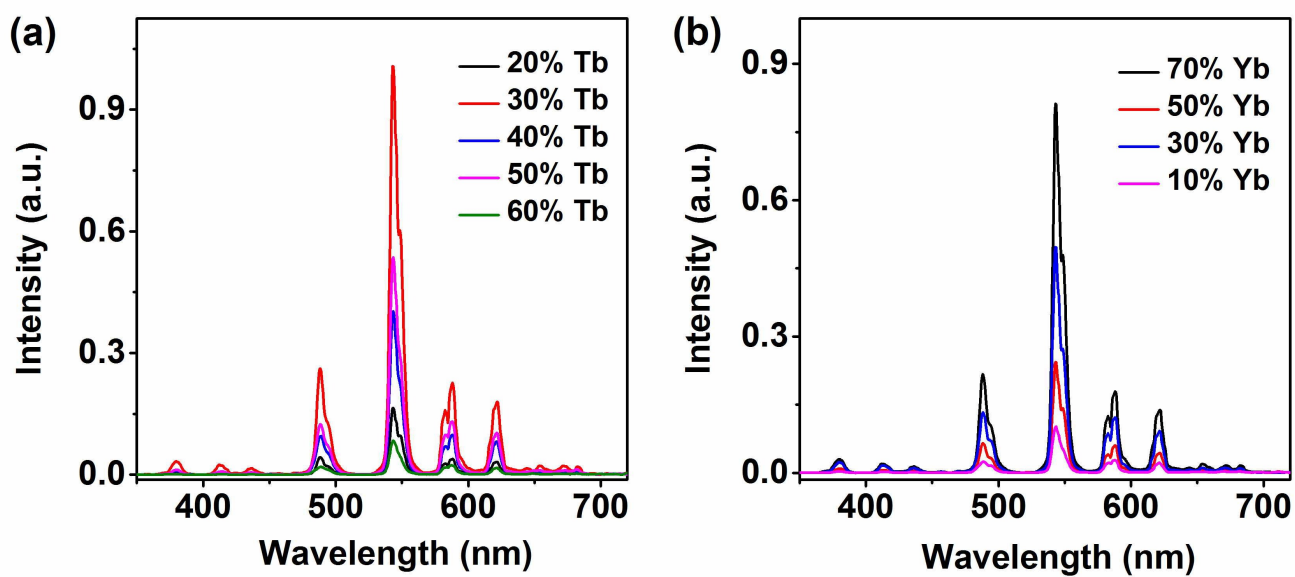
Figure S18. UCL spectra of (a) LiYbF$_4$:x%Tb and (b) LiYF$_4$:30%Tb, y%Yb UCNPs under 980-nm excitation. From the UCL spectra, the optimized Tb^{3+} concentration in LiYbF$_4$ was determined to be 30 mol%.
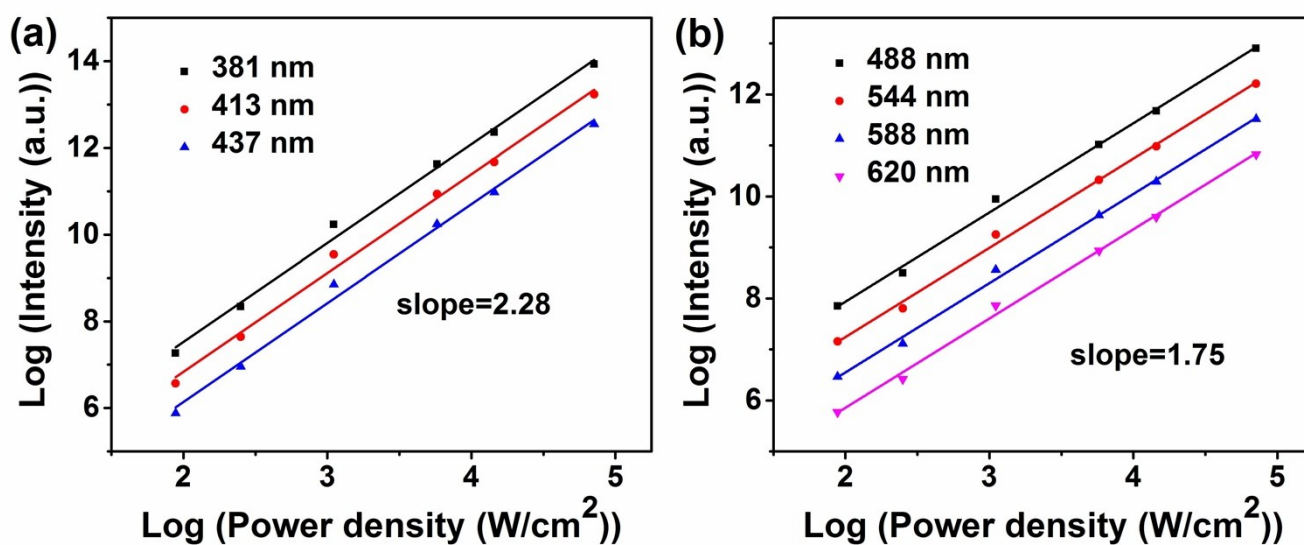
Figure S19. Log-log plots of the integrated UCL intensity versus 980-nm NIR excitation power density (W/cm²) for (a) $^5D_3 \rightarrow {}^7F_J$ (J=6, 5, 4) and (b) $^5D_4 \rightarrow {}^7F_J$ (J=6, 5, 4, 3) transitions of Tb^{3+}.
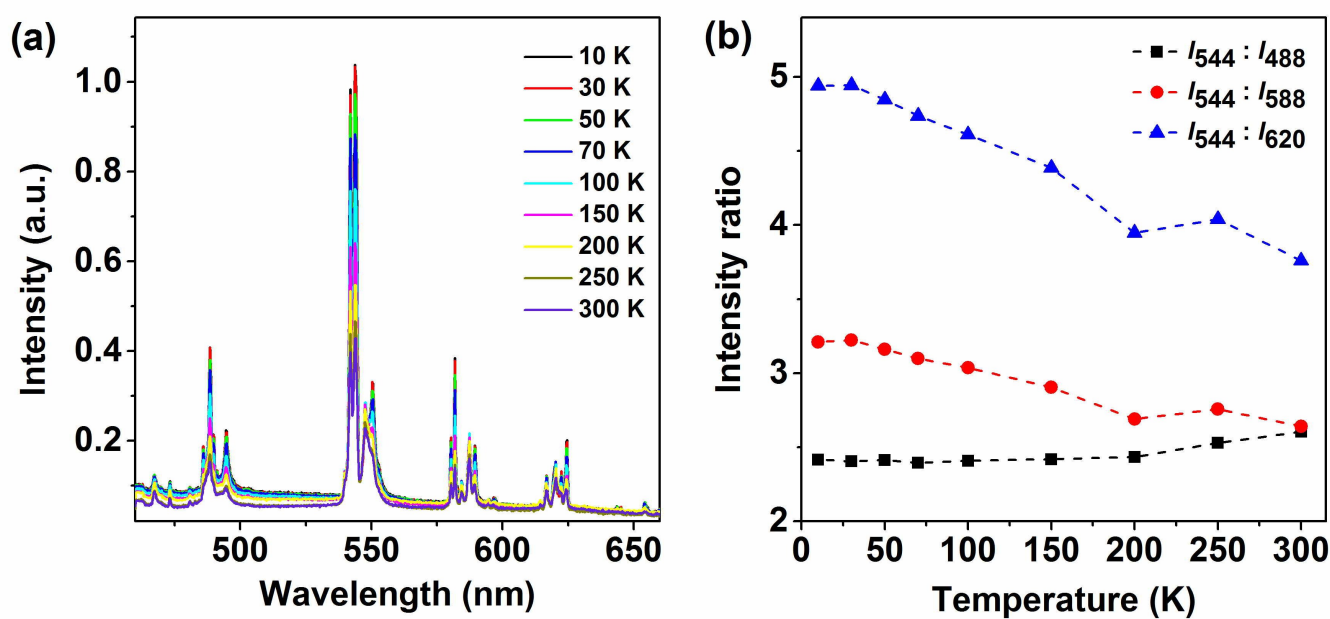
Figure S20. (a) Temperature-dependent DSL spectra of Tb^{3+} in $LiYbF_4{:}30\%Tb^{3+}@LiYF_4$ core/shell UCNPs under UV excitation at 368 nm. (b) Ratio of the integrated DSL intensities of $^5D_4 \rightarrow {}^7F_5$ (544 nm) to $^5D_4 \rightarrow {}^7F_6$ (488 nm), $^7F_4$ (588 nm), and $^7F_3$ (620 nm) transitions of Tb^{3+} as a function of temperature. The integrated DSL intensity of Tb^{3+} gradually decreases with the rise of temperature due to the larger non-radiative transition probability at higher temperature.
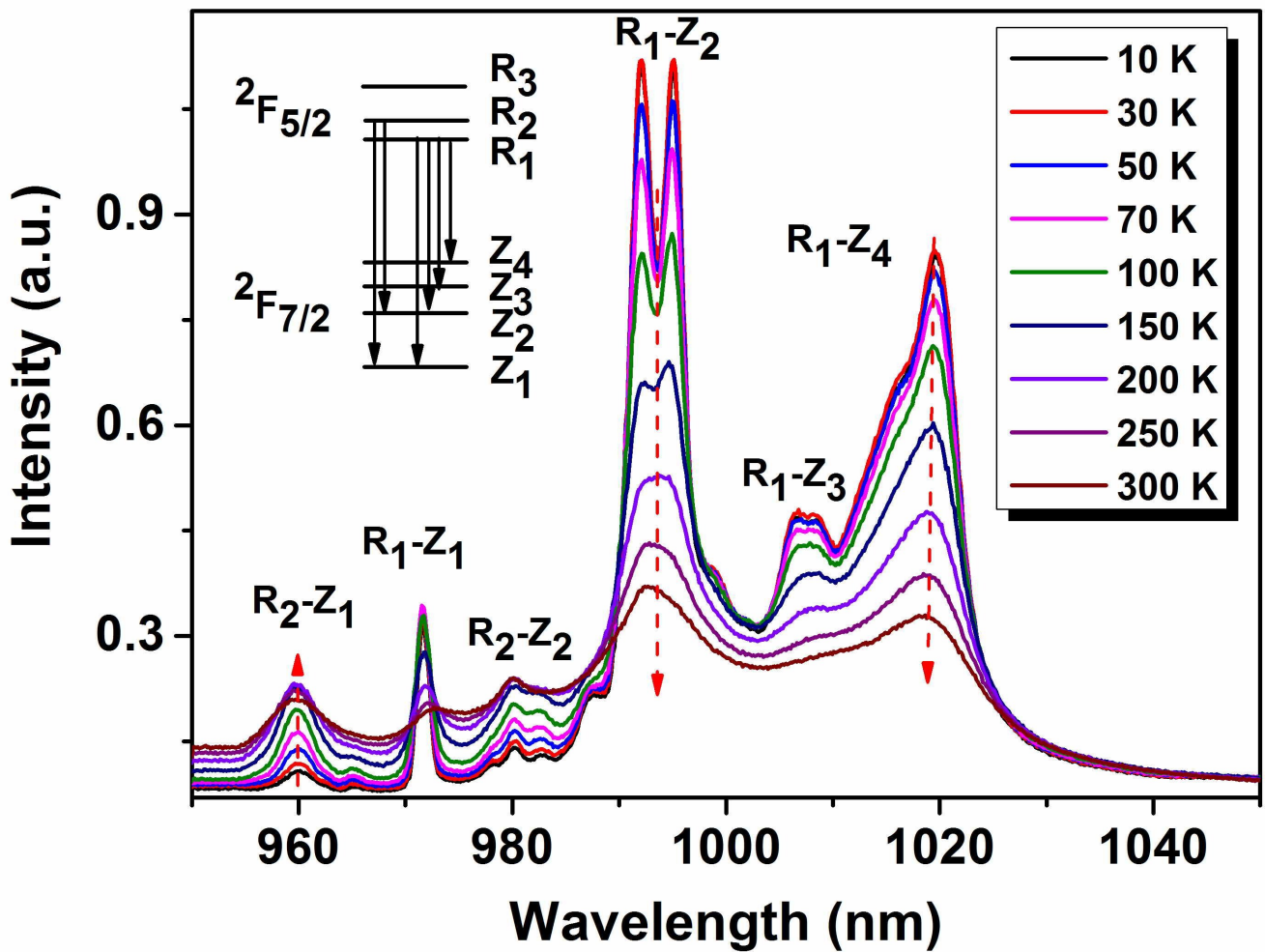
Figure S21. Temperature-dependent DSL spectra of Yb^{3+} in $LiYbF_4$:30%Tb^{3+}@$LiYF_4$ core/shell UCNPs under NIR excitation at 940 nm. The inset shows the Stark sub-levels of Yb^{3+} and the corresponding electronic transitions. The overall DSL intensity of Yb^{3+} gradually decreases with the rise of temperature due to the larger non-radiative transition probability at higher temperature. From the temperature-dependent DSL spectra, the lowest Stark sub-level of $^2F_{5/2}$ of Yb^{3+} was determined to be 10277 cm^{-1} (973 nm), assuming that all Yb^{3+} ions occupy a single site with a symmetry of S_4 in $LiYbF_4$.
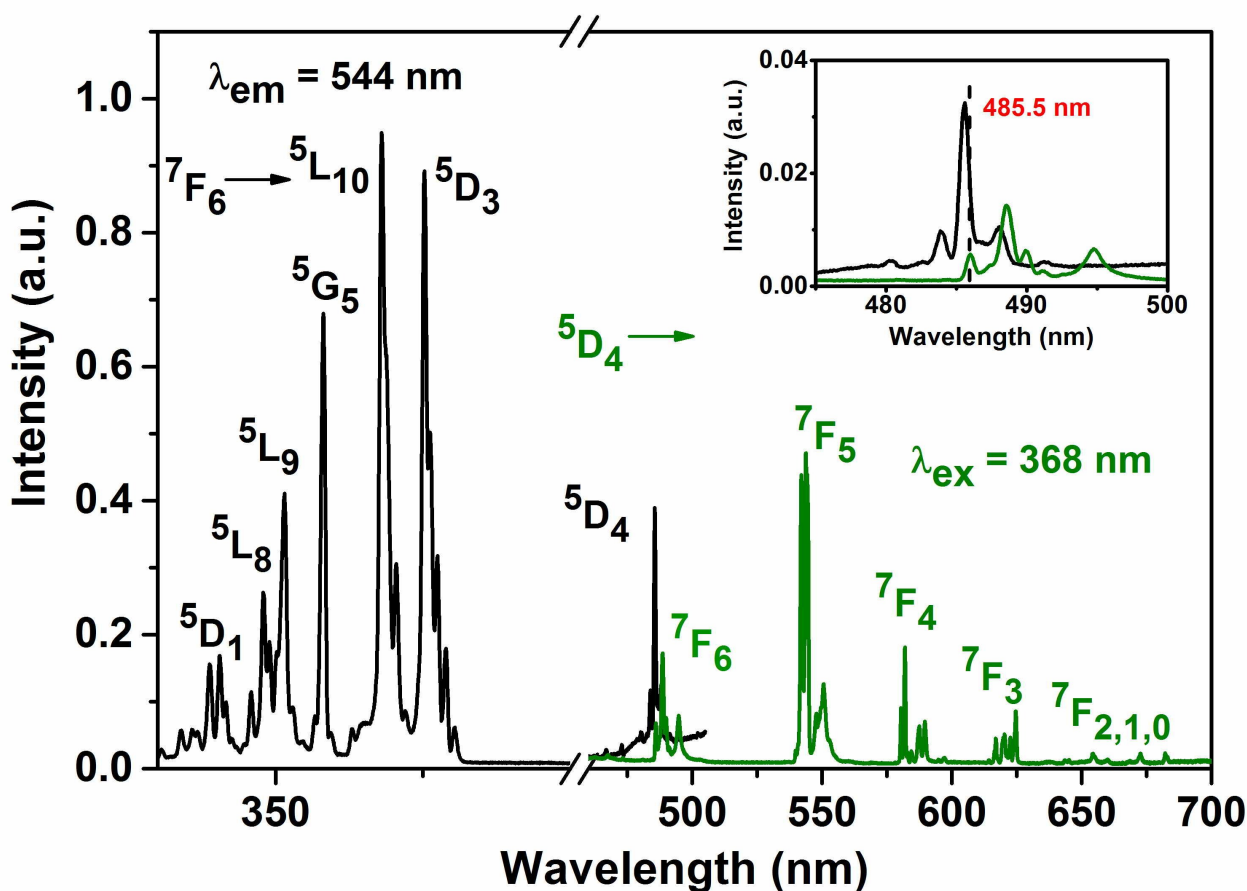
Figure S22. Low-temperature (10 K) and high-resolution (a) excitation and (b) emission spectra of Tb^{3+} in $LiYbF_4$:30%Tb^{3+}@$LiYF_4$ core/shell UCNPs. From the high-resolution PL spectra, the lowest Stark sub-level of $^5D_4$ of Tb^{3+} was determined to be 20597 cm^{-1} (485.5 nm), assuming that all Tb^{3+} ions occupy a single site with a symmetry of S_4 in $LiYbF_4$.
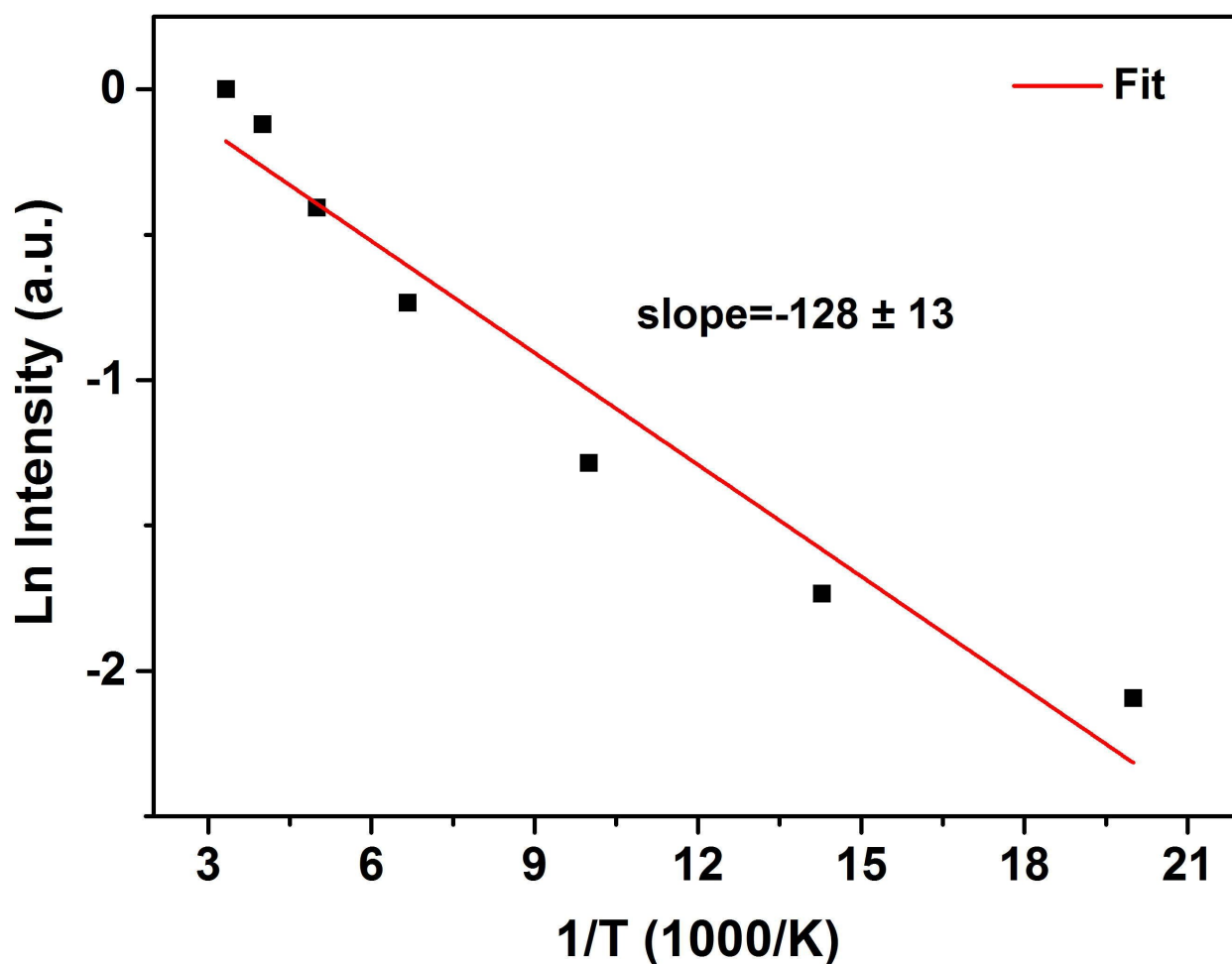
Figure S23. Arrhenius plot of the natural logarithm of normalized integrated UCL intensity *versus* the inverse of temperature. The solid line is a linear fit using Arrhenius equation: $\ln(I_t/I_0) = (-\Delta E)/(k_B T)$, where I_t represents the integrated UCL intensity of Tb^{3+} at temperature t, I_0 denotes the maximum integrated UCL intensity of Tb^{3+} at 300 K, ΔE is the UCL activation energy, k_B is Boltzmann's constant, and T is temperature. By linearly fitting the plot, ΔE was determined to be 128 ± 13 cm^{-1}, which is close to the energy mismatch (43 cm^{-1}) between the lowest Tb^{3+} $^5D_4$ level and twice the lowest Yb^{3+} $^2F_{5/2}$ level, thus verifying that the abnormal temperature-dependent UCL of Tb^{3+} is caused by phonon-assisted cooperative ET process.